AGU PUBLICATIONS

Geophysical Research Letters

RESEARCH LETTER
10.1002/2017GL074917

Key Points:
- The 3-D thermal structure of an ~8×10^7 m^3 block of ice in the Greenland ice sheet ablation zone was measured with over 300 sensors
- Unexpected horizontal temperature gradients are present across length scales below one ice thickness and through the full ice column
- Slow rates of diffusion relative to advective heat transfer can generate a heterogeneous temperature structure similar to what we observe

Supporting Information:
- Supporting Information S1
- Data Set S1

Correspondence to:
B. H. Hills,
benjamin.hills@umontana.edu

Citation:
Hills, B. H., Harper, J. T., Humphrey, N. F., & Meierbachtol, T. W. (2017). Measured horizontal temperature gradients constrain heat transfer mechanisms in Greenland ice. *Geophysical Research Letters*, *44*, 9778–9785. https://doi.org/10.1002/2017GL074917

Received 12 JUL 2017
Accepted 9 SEP 2017
Accepted article online 14 SEP 2017
Published online 5 OCT 2017

Measured Horizontal Temperature Gradients Constrain Heat Transfer Mechanisms in Greenland Ice

Benjamin H. Hills[1], Joel T. Harper[1], Neil F. Humphrey[2], and Toby W. Meierbachtol[1]

[1]Department of Geosciences, University of Montana, Missoula, MT, USA, [2]Department of Geology and Geophysics, University of Wyoming, Laramie, WY, USA

Abstract Ice in the ablation zone of the Greenland ice sheet is known to contain vertical temperature gradients that arise from conduction at the boundaries, the addition of strain and latent heat, and advective heat transport. A three-dimensional array of temperature measurements in a grid of boreholes reveals horizontal ice temperature gradients that challenge the present conceptualization of heat transfer. We measure two distinct types of temperature variability in the horizontal direction, one impacting a confined region where ice temperatures span a range of 5°C, and another with temperatures consistently varying by approximately 2°C across the entire 3-D block. We suggest the first demonstrates the localized and limited nature of latent heat input, and the second demonstrates that vertical heat advection outpaces diffusion. These findings imply that ice flow is highly variable over sub-ice-thickness length scales, which in turn generates contrasts in ice temperature that may impact ice deformation and fracturing.

1. Introduction

The temperature of ice has a first-order control on its viscosity (Hooke, 1981). Ice sheet temperature is thus fundamental to all aspects of flow dynamics including longitudinal stress transfer (e.g., Ryser et al., 2014), the onset of basal sliding (e.g., Brinkerhoff et al., 2011; MacGregor et al., 2016), and brittle failure (Schulson & Duval, 2009). At any given location in a moving ice sheet, the thermal structure reflects historical climate conditions and the integration of all upstream thermomechanical processes. Ice temperature is therefore a state variable that provides a robust modeling target (e.g., Lüthi et al., 2015; Meierbachtol et al., 2015; Poinar et al., 2016) and is one of the few measureable properties that give insight to the physical processes which control ice flow.

In the Greenland ice sheet (GrIS), various heat transfer processes warm ice as it moves hundreds of kilometers from the central accumulation zone to the low-elevation ablation zone. Heat is conducted into the ice from the upper and lower boundaries: the upper because of the relatively warm atmosphere and the lower due to a flux of geothermal heat (Petrunin et al., 2013; Shapiro & Ritzwoller, 2004) and sliding friction at the bed (Weertman, 1957). Internally, gravitational potential energy is transferred to heat as ice moves by deformation (van der Veen, 2013), and latent heat is added in discrete locations where water enters openings such as crevasses or moulins (e.g. Jarvis & Clarke, 1974; Phillips et al., 2010).

Measurements of ice temperature needed to confirm and constrain heat transfer processes in the GrIS ablation zone are rare. Nevertheless, a consistent vertical temperature structure has emerged from observations that consists of the coldest temperature located midway through the ice, and ice warming away from the cold core toward the surface and the bed (Harrington et al., 2015; Iken et al., 1993; Lüthi et al., 2015; Thomsen et al., 1991). Observations have thus far been insufficient to adequately constrain how this structure might change over the spatial scale of hundreds of meters to kilometers.

Here we reveal ice temperature gradients that also develop in the horizontal dimensions within the GrIS ablation zone; their presence providing insights into heat transfer processes. Our observational data set is based on temperature sensors installed in nine boreholes forming an instrumented block with sides equal to approximately one ice thickness. Within the block, we measure temperature gradients in all directions and the change in temperature over time. We use our observations to constrain advection-diffusion processes leading to advances in understanding of heat transfer in the ablation zone of the GrIS.

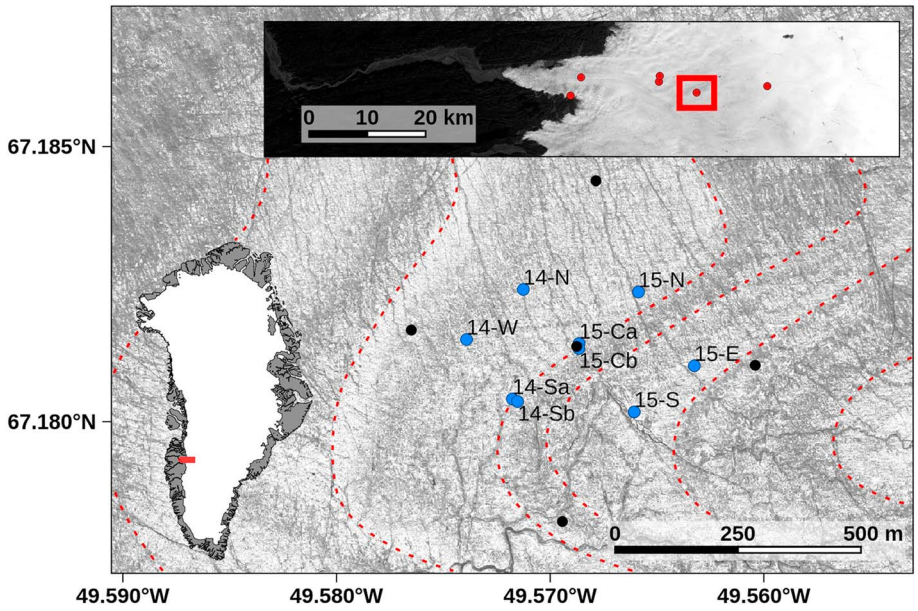

Figure 1. Map of the "block" field site showing five GPS stations (black) and nine boreholes (blue). Boreholes are named based on the year they were drilled and their cardinal direction from the center of the field site. The red dashed lines indicate foliations in the emerging dark ice layers seen in the WorldView-2 image. Inset: Location of the block site with respect to other drilling sites (Harrington et al., 2015) and the ice sheet margin, overlain on a Landsat image.

2. Methods

In 2014 and 2015 we drilled and instrumented nine boreholes to the bed of the GrIS at a site located 33 km from the terminus of Isunnguata Sermia in western Greenland (Figure 1 inset). The surface elevation of the site is 980 m, and the ice is 640–670 m deep. The nine boreholes are laid out in a double diamond grid (Figure 1) approximately 500 m E-W by 250 m N-S, all together forming an ~8×10^7 m^3 block of instrumented ice. Two boreholes were drilled within approximately 10 m of one another at the southwest and center locations.

Ice at this site moves up a slight reverse bed slope, and ice deformation measurements using tilt sensors indicate that motion is strongly dominated by basal sliding (Maier et al., 2016). High ablation rates (2–3 m/yr) result in small surface streams during summer, and the nearest moulin is 0.5 km south of the block. Foliated bands of dark, dust-filled ice (Wientjes & Oerlemans, 2010) emerge at the surface (Figure 1). These foliations have wavelengths from 0.5 to 2 km and horizontal amplitudes from hundreds of meters to kilometers.

The instrumented block of ice is equipped with a total of 313 temperature sensors distributed in the nine profiles. Sensors are spaced at 10 m in the ~150 m of ice closest to the bed and 20 m above. We use TMP102 temperature sensors that have 12 bit analog-to-digital converters with resolution 0.0625°C. Immediately after drilling, liquid water temperatures were measured within the borehole. Those initial measurements are used as a melting point calibration to increase accuracy; hence, we are confident in the temperature measurements to within ±0.1°C. Measurements are made with custom built data loggers installed at the ice surface, typically at a 4 h time interval.

Hot water drilling creates a thermal disturbance in the ice. Over the 2 to 3 months following drilling, the measured ice temperatures throughout each profile show asymptotic cooling to a stable temperature following the expected time scale based on theory (Humphrey & Echelmeyer, 1990, equation (24)). Therefore, the temperatures presented here, measured either 1 or 2 years after the drilling date (many months after cooling ceases), are representative of the actual ice temperature within less than one step in the sensor resolution.

Temperature profiles through the ice can be plotted in various ways, such as referenced to the ice surface, the bed surface, or relative to elevation above sea level. Our block has irregular bed topography and a sloping ice surface that does not mimic the bed. We therefore represent the temperature field and its gradients with

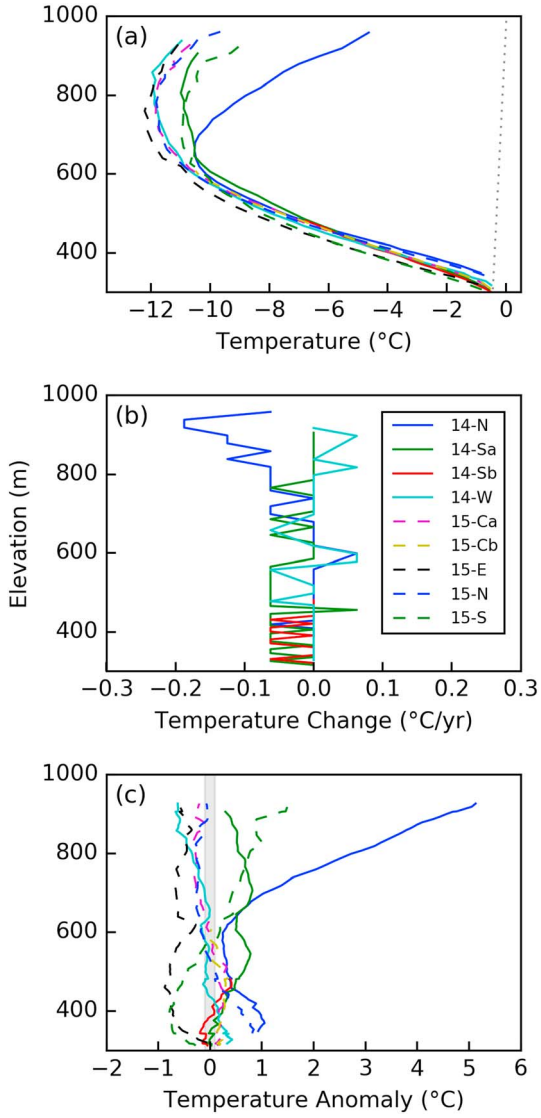

Figure 2. (a) Temperature profiles from the instrumented block (colored) and the pressure-dependent melting point (gray). (b) Temperature change over 1 year for profiles with measurements in the summers of both 2015 and 2016. One step in the sensor resolution is 0.0625°C. (c) Spatial variability of ice temperature plotted as the anomaly from a mean profile. Variations are measured across equal elevation bands; all ice at the bed is temperate, but variations exist near 300 m elevation due to unequal bed elevations. The shaded region is the range in sensor accuracy, ±0.1°C.

respect to elevation. The surface elevation is determined from high-resolution GPS measurements, the total ice depth is known to within <1.5% from borehole drilling (Wright et al., 2016), and the installation location of each sensor within the ice column is constrained to about 0.25 m.

3. Results

The vertical temperature structure of our instrumented block follows the expected pattern of coldest temperature approximately midway through the ice depth (Figure 2a). The ice at the bed is at the melting point, with a thin layer of temperate basal ice up to ~5 m thick. Some of the temperature profiles have no temperate measurement because there is no sensor close enough to the bed to measure temperate ice. In those cases, we are confident that the bed is in fact temperate based on measured pressure variations in a layer of liquid water (Wright et al., 2016). Above the warm basal layer, ice becomes colder following a roughly linear temperature gradient of about −0.04°C/m until the coldest temperatures of about −10 to −12°C, between 200 and 300 m below the ice surface. Above the cold core, ice becomes warmer toward the surface following a gradient of about +0.01°C/m.

Despite their proximity, no two temperature profiles in the 3-D block match one another. In many cases, the disparities between profiles reveal temperature gradients in the horizontal direction that are clearly distinguishable from measurement error. Other temperature profiles we have measured in closely spaced boreholes at sites located 6 km down glacier and 13 km up glacier also demonstrate similar variability (Harrington et al., 2015). In this study, the horizontal temperature gradients can be classified into two distinct types.

The first type is a highly confined but very large-amplitude thermal anomaly impacting a select package of ice surrounding just one borehole (Figure 2a, hole 14-N). Near the surface, the temperature profile of 14-N is more than 5°C warmer than other profiles in the block. No distinguishable manifestation of the thermal anomaly is present in other profiles, including the closest one located only 150 m away. The horizontal temperature gradient between this profile and its neighbors is up to ~0.033°C/m, close to the magnitude of the steepest vertical gradients we observe, 0.04°C/m. Yet the warm anomaly attenuates with depth, and the profile of 14-N begins to resemble the mean temperature of other profiles about 350 m below the surface.

Time series data show a slow loss of heat from the anomalously warm region of 14-N from 2015 to 2016 (Figure 2b). The maximum cooling rate was ~0.2°C/yr, observed near the surface. During this same time interval, other boreholes in the block demonstrate no change in temperature above the resolution of the measurements.

The second type of horizontal temperature gradient extends among all boreholes of the block. Disregarding the warm anomaly confined to the top half of 14-N, all eight remaining profiles demonstrate temperatures that vary at any given elevation by up to ±1°C about the mean (Figure 2c). These horizontal temperature gradients are on the order of ~0.01°C/m, which results in heat flux of up to 0.021 W/m^2. These horizontal fluxes are about two thirds of the estimated geothermal heat flux at the bed in this region (Meierbachtol et al., 2015).

Overall, the horizontal temperature field has no discernible spatial pattern (Figure 3). This second type of horizontal temperature gradient extends through the full thickness of the ice, unlike the confined type described

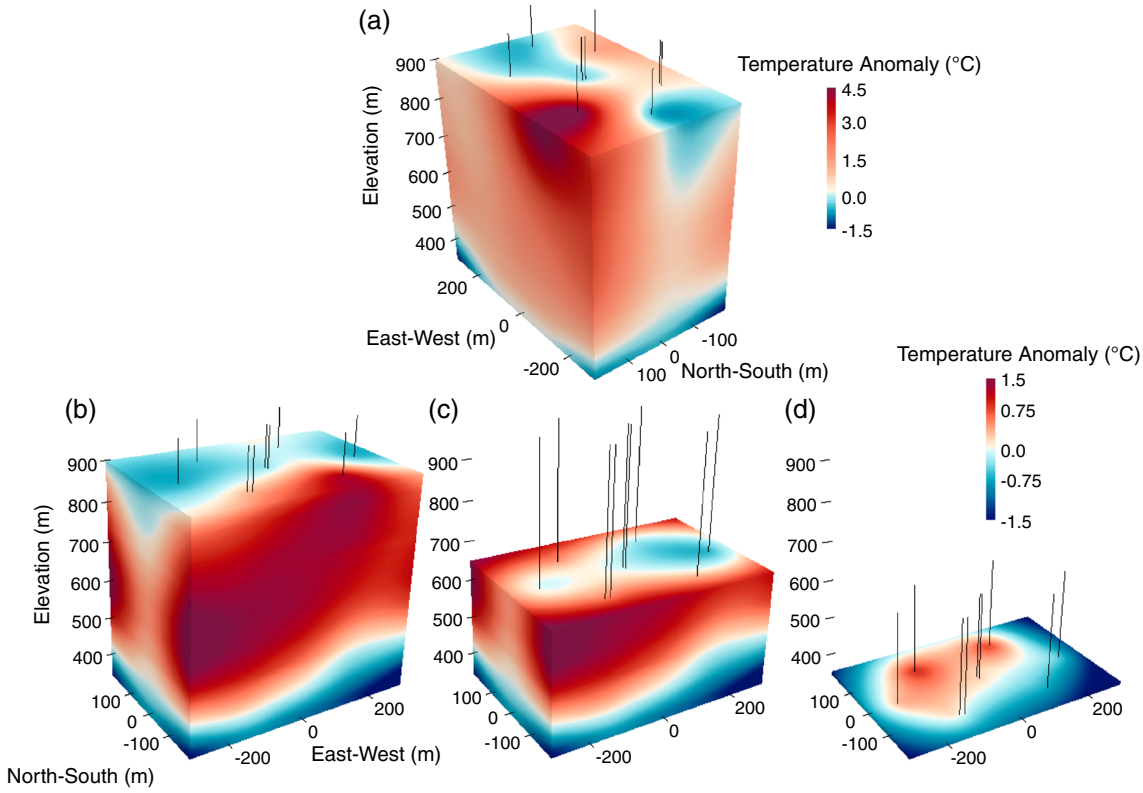

Figure 3. Three-dimensional visualizations of the two types of observed horizontal temperature gradients within the instrumented ice block. Temperatures are interpolated between the measured values using a radial basis function, and values are plotted as the anomaly from the mean temperature profile (as in Figure 2c). Vertical lines show borehole locations. (a) Visualization of the confined warming near borehole 14-N. (b–d) Visualizations of the unstructured nature of horizontal temperature gradients at various depths. Each of these blocks represents the same temperature field with the top portion removed by a slice at 900 m (Figure 3b), 650 m (Figure 3c), and 350 m (Figure 3d). The confined anomaly is excluded from Figures 3b–3d to highlight gradients unrelated to that feature. Note that the scale bar for Figures 3b–3d is different from that for Figure 3a.

above. In some cases, the gradients between two individual profiles reverse at depth with heat flowing laterally one direction near the surface and the opposite direction closer to the bed. Nevertheless, the 2°C range between different temperature profiles is relatively consistent with depth. We know that the horizontal gradients are not simply a plotting artifact, as they exist similarly in every coordinate reference frame (i.e., bed referenced, surface referenced, geoid referenced, and relative depth referenced, see Figure S1 in the supporting information).

4. Discussion

4.1. Confined Warming

Our data identify a region of confined and anomalous warming, with one profile that is highly altered from the eight others in the block and from all others measured in the region (Harrington et al., 2015). Despite the sparsity of temperature profiles previously collected in the GrIS ablation zone, a very similar warm anomaly has been documented elsewhere. Two profiles from one field site in the Pakitsoq region located 100 m apart demonstrated temperature profiles that differ in the upper 300 m by up to 5°C (Lüthi et al., 2015), nearly identical circumstances to ours. This suggests that anonymously warm packages in the top half of the ice sheet may not be uncommon. Their potential causes and impacts on bulk ice temperature thus warrant consideration.

As with Lüthi et al. (2015), we hypothesize that latent heat is the only viable source for this warm anomaly. In fact, close to the borehole, we observed an exposed feature that appears to be a refrozen crevasse (Figure S2). Furthermore, a simple calculation shows that only ~3% refrozen water by volume could produce the measured anomaly (supporting information section S2). A remaining source of puzzlement, however, is

the means by which water can penetrate halfway through the ice sheet, but no farther. Lüthi et al. (2015) suggest that hydrofracturing injected water to depth, but penetration was limited to the upper few hundred meters because the fracture could not propagate into warmer ice below the cold central core. An alternative explanation is that the warm anomaly is associated with an old moulin and the old crevasse we see at the surface is unrelated. A moulin could divert away from the measured temperature profile at depth, since moulins sometimes undergo horizontal jogs (Holmlund, 1988; Vatne, 2001). Regardless, a discrete package of latent heat seems the most likely source for such a local and high-magnitude temperature offset and is consistent with previous observations.

While locally important, the overall impact of such features on bulk ice temperature appears quite limited. Despite the large contrast with surrounding ice temperature, our data show that the warm anomaly has a relatively slow rate of heat transfer to surrounding ice. We can verify the persistent nature of the thermal anomaly with a characteristic diffusion length scale, $r = 2\sqrt{\kappa t}$, where κ is the thermal diffusivity of ice and t is time (Carslaw & Jaeger, 1959). Based on this length scale, warm ice remains confined to within hundreds of meters from the source (Figure S3), even after one thousand years have elapsed. Since the mean density of moulins in this region of the ice sheet is on the order of 0.1 moulin/km^2 (Smith et al., 2015), more than 60,000 years are required to achieve thermal overlap between evenly spaced moulins—much longer than the residence time of ice in this area. Such latent heating events thus create strong localized and persistent horizontal temperature gradients but do little for bulk warming of the ice.

4.2. Full-Depth Horizontal Gradients

Two key constraints from observations make it unlikely that the horizontal gradients across our three-dimensional data set (aside from the confined warming above) can be attributed to latent heating. First is that these gradients are nearly uniform across the full thickness of the ice. Hence, latent heat would somehow need to be injected all the way through the ice to induce the full-depth temperature variability. Studies have shown that full-depth fracturing occurs only in rare circumstances where surface lake draining promotes hydrofracturing, and the fracture opening quickly becomes a moulin (Das et al., 2008; Doyle et al., 2013). If surface and basal fractures were to penetrate only partway, the diffusion time scale for ice is far too long to conduct heat to the central cold core (supporting information section S4). Furthermore, surface ablation at meters per year will quickly remove any warm ice packages that result from latent heating at the surface.

A second and important constraint stems from the horizontal pattern of the observed temperature gradients, namely, the lack of any consistent direction to these gradients and their tendency to sometimes change direction with depth. To create the gradients with latent heat sources, a highly complex arrangement of numerous water sources would be required. Those water sources would need to vary in both horizontal and vertical space. Such an arrangement seems unlikely. Furthermore, similar horizontal temperature variability was observed between two or three boreholes at three other sites we have drilled many kilometers away, both up glacier and down glacier (Harrington et al., 2015). While the spread of those profiles is smaller and somewhat different to what we observe within the block, the horizontal spacing between them is also much smaller. These measurements therefore suggest that this type of gradient is widespread across the ablation zone.

4.2.1. Variable Vertical Advection

We postulate an alternative explanation for sub-ice-thickness scale temperature variability stemming from the flow history of ice, rather than variability of heat sources. Ice in the ablation zone flows over a rough bed with topographic relief that, in places, includes ridges and troughs with amplitudes of hundreds of meters (Lindbäck & Pettersson, 2015), a significant fraction of the ice depth. Additionally, the surface of the ice is removed by ablation at tens of meters per decade, or, equivalently, tens of meters per kilometer of marginward displacement. Foliations visible on the ice surface are created by the irregular emergence of distorted internal layers (Figures 1 and S6). The complex flow history likely moves energy in a spatially variable way, which could potentially generate the horizontal temperature gradients that we observe. Horizontal temperature gradients will only develop, however, if the rate of vertical offset outpaces the tendency of heat diffusion to equilibrate the gradients.

To explore this conceptualization, we employ an advection-diffusion model simulating vertical offset of initial temperature profiles from ice flow with simultaneous heat diffusion. Importantly, our objective here is to test the characteristic impacts of vertical advection and diffusion processes, rather than simulate our block or

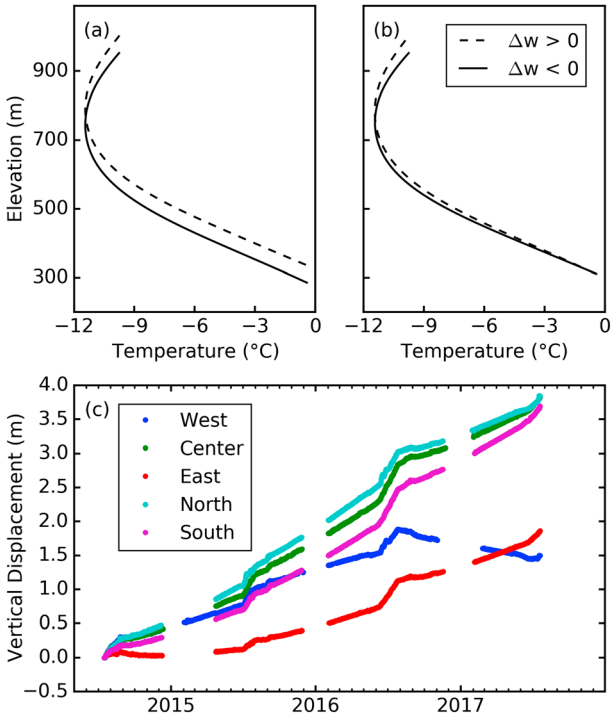

Figure 4. Temperature profiles from two advection-diffusion simulations: (a) bed-parallel flow and (b) vertical strain. The results are shown after 50 years of advection-diffusion at two locations separated by 350 m horizontal distance, one with upward velocity and the other downward. (c) Cumulative vertical displacement measured over 3 years at five GPS stations on the ice surface.

replicate our measured temperature profiles. Our five GPS stations surrounding the 3-D block demonstrate that the surface displacement can vary by about 1 m/yr across the block (Figure 4c and supporting information section S5). We create an artificial field of vertical velocity variations that is sinusoidal in nature with amplitude 0.5 m/yr, based on GPS observations, and wavelength 700 m, based on both foliations and GPS observations. Vertical surface motion results from bed-parallel flow and vertical strain. We consider the effects of each of these individually over a 50-year time frame, such that (a) all vertical motion observed at the surface results from bed-parallel flow so that vertical velocities are constant through the ice column, and (b) vertical strain rates are uniform so that the vertical velocity is linear through the column and zero at the bed. A horizontal component of flow is included to conserve mass in the constant-strain scenario (see supporting information section S6 for model details).

The simulations demonstrate that differential vertical flow can produce and preserve temperature offsets between nearby vertical profiles with a magnitude and pattern similar to what we observe (Figure 4). Both cases cause offsetting, but only the bed-parallel flow case yields offset temperature profiles across the full ice depth including the bottom half of the ice column as observed. A reversal of the offset direction at depth occurs in this scenario too, as some of our profiles also demonstrate. Observations of ice deformation within the ablation zone support that the majority of ice flow is sliding (Maier et al., 2016; Ryser et al., 2014), so it is likely that vertical motion is dominated by bed-parallel flow.

Our simplified simulations isolate the competition between advective and diffusive heat transfer in two end-member scenarios. In a more realistic scenario, the vertical flow is time-space variable, and ablation continuously removes ice at the surface, resetting the location of the surface boundary. The cumulative history of vertical flow and ablation within our study block is unknowable and cannot be reconstructed in a model simulation. Nevertheless, our results do demonstrate that this mechanism can produce local horizontal temperature variability of the magnitude and pattern we observe. With no alternative explanation available, we find this to be the most plausible process generating the horizontal gradients.

A scaling argument can be used to constrain the possible effectiveness of this mechanism within the GrIS ablation zone. The rate of advective heat transfer promoting the growth of horizontal temperature gradients is $\Delta w \frac{\partial T}{\partial z}$ (where Δw is the change in vertical velocity between two nearby columns of ice). However, horizontal diffusion acts to remove temperature variations. Consider temperatures that vary periodically in the horizontal direction, $\overline{T} = Ae^{i\frac{2\pi}{\lambda}x}$, where $\overline{T}$ is the temperature variation from the mean, A is the amplitude, and λ is the wavelength of periodic variations. In this case, diffusion removes gradients at a rate equal to the diffusivity of ice times the second derivative in the horizontal direction, which is $-\kappa A\left(\frac{2\pi}{\lambda}\right)^2$. Even small wavelengths of less than one ice thickness are capable of muting the effects of horizontal diffusion. Therefore, in cases with some amount of vertical velocity variation, heat transport by diffusion is likely slower than that by advection, allowing horizontal temperature gradients to develop. However, because the vertical velocity variations are unsteady, sub-ice-thickness scale temperature variability is likely limited to a few degrees at most (supporting information section S7).

4.3. Implications

The complex thermal structure we observe likely plays a key role in ice flow dynamics of the ablation zone. The rate factor, $A(T)$, in Glen's law is exponentially dependent on temperature (Hooke, 1981). Assuming an activation energy of 78.8 kJ/mol K (van der Veen, 2013), the 2°C horizontal temperature variability we observe corresponds to changes in the rate factor by about 30% at these temperatures. Likewise, the confined thermal anomaly, which is up to 5°C warmer than surrounding ice, represents roughly a doubling of the rate

factor. Small changes in viscosity are expected to have a large influence on longitudinal coupling due to high flow rates in the ablation zone (Ryser et al., 2014). Additionally, prior measurements have shown that the internal deformation field in Greenland ice can be highly variable in time and space (Ryser et al., 2014), which may in part be related to local ice temperature variability.

Temperature also controls the propensity for fracture propagation. The critical crack tip loading rate is exponentially dependent on temperature (Schulson & Duval, 2009, Table 9.1). This means that variability in ice temperature alters the mechanics of fracture in ice and temperature gradients could divert or arrest the propagation of a fracture. Consideration of horizontal temperature variability may thus be important to modeling the details of lake drainage events or calving dynamics.

5. Conclusions

Our three-dimensional measurements in nine full-depth boreholes show vertical and horizontal temperature gradients in the GrIS ablation zone. The horizontal gradients are unexpected and can be categorized into two types: a +5°C anomaly confined to the upper 300 m of ice depth in a limited area of the study block and temperature variability over a 2°C range extending through the full ice thickness. The confined warming likely owes its origins to a discrete latent heating event that is slow to diffuse away. The full-depth temperature variability may be the result of locally variable rates of vertical heat advection related to ice flow over large bedrock bumps.

Our observational data demonstrate that the slow rate of diffusion in ice leads to a largely variable thermal structure in the horizontal as well as vertical directions, even at the sub-ice-thickness scale. Heat transfer processes of latent heating and advection act over short length scales and shorter time scales than diffusion, enabling the establishment of these gradients. The complex thermal structure has implications for flow dynamics, as well as the interpretation of other temperature observations with regard to our understanding of physical processes in the ice sheet.

Acknowledgments
This work was funded by the National Science Foundation (Office of Polar Programs-Arctic Natural Sciences grant 1203451). We thank Douglas Brinkerhoff and one anonymous reviewer for their valuable input and critiques on an earlier version of this manuscript. All temperature data used in this study are available with the supporting information.

References

Brinkerhoff, D. J., Meierbachtol, T. W., Johnson, J. V., & Harper, J. T. (2011). Sensitivity of the frozen/melted basal boundary to perturbations of basal traction and geothermal heat flux: Isunnguata Sermia, western Greenland. *Annals of Glaciology*, *52*(59), 43–50. https://doi.org/10.3189/172756411799096330

Carslaw, H. S., & Jaeger, J. C. (1959). *Conduction of Heat in Solids* (2nd ed.). London: Oxford Univ. Press.

Das, S. B., Joughin, I. R., Behn, M. D., Howat, I. M., King, M. A., Lizarralde, D., & Bhatia, M. P. (2008). Fracture propagation to the base of the Greenland ice sheet during supraglacial lake drainage. *Science*, *320*(5877), 778–781.

Doyle, S. H., Hubbard, A. L., Dow, C. F., Jones, G. A., Fitzpatrick, A., Gusmeroli, A., … Box, J. E. (2013). Ice tectonic deformation during the rapid in situ drainage of a supraglacial lake on the Greenland ice sheet. *The Cryosphere*, *7*(1), 129–140. https://doi.org/10.5194/tc-7-129-2013

Harrington, J. A., Humphrey, N. F., & Harper, J. T. (2015). Temperature distribution and thermal anomalies along a flowline of the Greenland ice sheet. *Annals of Glaciology*, *56*(70), 98–104. https://doi.org/10.3189/2015AoG70A945

Holmlund, P. (1988). Internal geometry and evolution of moulins, Storglaciären, Sweden. *Journal of Glaciology*, *34*(117), 242–248.

Hooke, R. L. (1981). Flow law for polycrystalline ice in glaciers: Comparison of theoretical predictions, laboratory data, and field measurements. *Reviews of Geophysics*, *19*, 664–672. https://doi.org/10.1029/RG019i004p00664

Humphrey, N., & Echelmeyer, K. (1990). Hot-water drilling and bore-hole closure in cold ice. *Journal of Glaciology*, *36*(124), 287–298. https://doi.org/10.3189/002214390793701354

Iken, A., Echelmeyer, K., Harrison, W., & Funk, M. (1993). Mechanisms of fast flow in Jakobshavns Isbrae, West Greenland: Part I. Measurements of temperature and water level in deep boreholes. *Journal of Glaciology*, *39*(131), 15–25.

Jarvis, G. T., & Clarke, G. K. C. (1974). Thermal effects of crevassing on Steele Glacier, Yukon Territory, Canada. *Journal of Glaciology*, *13*(68), 243–254.

Lindbäck, K., & Pettersson, R. (2015). Spectral roughness and glacial erosion of a land-terminating section of the Greenland ice sheet. *Geomorphology*, *238*, 149–159. https://doi.org/10.1016/j.geomorph.2015.02.027

Luthi, M., Funk, M., Iken, A., Gogineni, S., & Truffer, M. (2002). Mechanisms of fast flow in Jakobshavns Isbræ, West Greenland: Part III. Measurements of ice deformation, temperature and cross-borehole conductivity in boreholes to the bedrock. *Journal of Glaciology*, *48*(162), 369–385.

Lüthi, M. P., Ryser, C., Andrews, L. C., Catania, G. A., Funk, M., Hawley, R. L., … Neumann, T. A. (2015). Heat sources within the Greenland ice sheet: Dissipation, temperate paleo-firn and cryo-hydrologic warming. *The Cryosphere*, *9*(1), 245–253. https://doi.org/10.5194/tc-9-245-2015

MacGregor, J. A., Fahnestock, M. A., Catania, G. A., Aschwanden, A., Clow, G. D., Colgan, W. T., … Seroussi, H. (2016). A synthesis of the basal thermal state of the Greenland ice sheet. *Journal of Geophysical Research: Earth Surface*, *121*, 1328–1350. https://doi.org/10.1002/2015JF003728

Maier, N. T., Humphrey, N. F., Harper, J. T., & Meierbachtol, T. W. (2016). Measured deformation enhancement in western Greenland shows the importance of viscosity reduction for elevated melt season velocities, AGU Fall Meeting C33A-0770.

Meierbachtol, T. W., Harper, J. T., Johnson, J. V., Humphrey, N. F., & Brinkerhoff, D. J. (2015). Thermal boundary conditions on western Greenland: Observational constraints and impacts on the modeled thermomechanical state. *Journal of Geophysical Research: Earth Surface*, *120*, 623–636. https://doi.org/10.1002/2014JF003375

Petrunin, A. G., Rogozhina, I., Vaughan, A. P. M., Kukkonen, I. T., Kaban, M. K., Koulakov, I., & Thomas, M. (2013). Heat flux variations beneath central Greenland's ice due to anomalously thin lithosphere. *Nature Geoscience*, *6*(9), 746–750. https://doi.org/10.1038/ngeo1898

Phillips, T., Rajaram, H., & Steffen, K. (2010). Cryo-hydrologic warming: A potential mechanism for rapid thermal response of ice sheets. *Geophysical Research Letters*, *37*, L20503. https://doi.org/10.1029/2010GL044397

Poinar, K., Joughin, I., Lenaerts, J. T. M., & van den Broeke, M. R. (2016). Englacial latent-heat transfer has limited influence on seaward ice flux in western Greenland. *Journal of Glaciology*, *63*, 1–16. https://doi.org/10.1017/jog.2016.103

Ryser, C., Lüthi, M. P., Andrews, L. C., Catania, G. A., Funk, M., Hawley, R., … Neumann, T. A. (2014). Caterpillar-like ice motion in the ablation zone of the Greenland ice sheet. *Journal of Geophysical Research: Earth Surface*, *119*, 2258–2271. https://doi.org/10.1002/2013JF003067

Schulson, E. M., & Duval, P. (2009). *Creep and fracture of ice*. Cambridge, UK: Cambridge University Press.

Shapiro, N. M., & Ritzwoller, M. H. (2004). Inferring surface heat flux distributions guided by a global seismic model: Particular application to Antarctica. *Earth and Planetary Science Letters*, *223*(1–2), 213–224. https://doi.org/10.1016/j.epsl.2004.04.011

Smith, L. C., Chu, V. W., Yang, K., Gleason, C. J., Pitcher, L. H., Rennermalm, A. K., … Balog, J. (2015). Efficient meltwater drainage through supraglacial streams and rivers on the southwest Greenland ice sheet. *Proceedings of the National Academy of Sciences of the United States of America*, *112*(4), 1001–1006. https://doi.org/10.1073/pnas.1413024112

Thomsen, H. H., Olesen, O. B., Braithwaite, R. J., & Bøggild, C. E. (1991). Ice drilling and mass balance at Pakitsoq, Jakobshavn, central West Greenland. *Report Geology Survey Greenland*, *152*, 80–84.

Vatne, G. (2001). Geometry of englacial water conduits, Austre Brøggerbreen, Svalbard. *Norsk Geografisk Tidsskrift - Norwegian Journal of Geography*, *55*(2), 85–93. https://doi.org/10.1080/713786833

van der Veen, C. J. (1998). Fracture mechanics approach to penetration of surface crevasses on glaciers. *Cold Regions Science and Technology*, *27*, 31–47.

van der Veen, C. J. (2013). *Fundamentals of Glacier Dynamics* (2nd ed.). Boca Raton, FL: CRC Press.

Weertman, J. (1957). On the sliding of glaciers. *Journal of Glaciology*, *3*(21), 33–38.

Wientjes, I. G. M., & Oerlemans, J. (2010). An explanation for the dark region in the western melt zone of the Greenland ice sheet. *The Cryosphere*, *4*(3), 261–268. https://doi.org/10.5194/tc-4-261-2010

Wright, P. J., Harper, J. T., Humphrey, N. F., & Meierbachtol, T. W. (2016). Measured basal water pressure variability of the western Greenland ice sheet: Implications for hydraulic potential. *Journal of Geophysical Research: Earth Surface*, *121*, 1134–1147. https://doi.org/10.1002/2016JF003819